http://doi.org/10.35784/iapgos.7826 *received: 28.05.2025 | revised: 02.01.2026 | accepted: 26.01.2026 | available online: 30.03.2026*

INTELLIGENT DL-SCH/PDSCH PROCESSING CHAIN IN 5G WITH ADAPTIVE HARQ MECHANISM

Juliy Boiko[1], Ilya Pyatin[2]
[1]Khmelnytskyi National University, Department of Telecommunications, Media and Intelligent Technologies, Khmelnytskyi, Ukraine, [2]Khmelnytskyi Polytechnic Professional College by Lviv Polytechnic National University, Department of Computer Engineering, Khmelnytskyi, Ukraine

Abstract. *The article presents the design and analysis of an intelligent processing chain for the Downlink Shared Channel (DL-SCH) and the Physical Downlink Shared Channel (PDSCH) with an adaptive Hybrid Automatic Repeat Request (HARQ) mechanism for fifth-generation (5G) wireless networks. The study integrates machine learning techniques to optimize the HARQ retransmission process, thereby enhancing system throughput, latency, and energy efficiency. Experimental results compare the proposed system with a conventional HARQ mechanism across various signal-to-noise ratio (SNR) levels, demonstrating throughput improvements of up to 72.5% and latency reduction of up to 23% under low-to-moderate SNR conditions. The findings highlight the potential of adaptive HARQ schemes for future fifth- and sixth-generation (5G and 6G) communication systems. System performance was evaluated in terms of bit error rate (BER), error vector magnitude (EVM), modulation error ratio (MER), and power efficiency, with an emphasis on real-time adaptability and system-level quality of service (QoS) requirements.*

Keywords: 5G networks, automatic repeat request, signal-to-noise ratio, intelligent control

INTELIGENTNY ŁAŃCUCH PRZETWARZANIA DL-SCH/PDSCH W SIECI 5G Z ADAPTACYJNYM MECHANIZMEM HARQ

Streszczenie. *W artykule przedstawiono projekt oraz analizę inteligentnego łańcucha przetwarzania dla kanału współdzielonego łącza w dół (Downlink Shared Channel, DL-SCH) oraz fizycznego kanału współdzielonego łącza w dół (Physical Downlink Shared Channel, PDSCH) z adaptacyjnym mechanizmem hybrydowej automatycznej retransmisji (Hybrid Automatic Repeat Request, HARQ) przeznaczonym dla sieci piątej generacji (5G). W badaniach zastosowano techniki uczenia maszynowego w celu optymalizacji procesu retransmisji HARQ, co pozwala na zwiększenie przepustowości systemu, redukcję opóźnień oraz poprawę efektywności energetycznej. Wyniki eksperymentalne obejmują porównanie proponowanego rozwiązania z konwencjonalnym mechanizmem HARQ dla różnych poziomów stosunku sygnału do szumu (SNR), wykazując wzrost przepustowości sięgający 72,5% oraz skrócenie opóźnień do 23% w warunkach niskiego i umiarkowanego SNR. Uzyskane rezultaty potwierdzają potencjał adaptacyjnych mechanizmów HARQ w przyszłych systemach komunikacyjnych piątej i szóstej generacji (5G i 6G). Wydajność systemu oceniono pod kątem współczynnika błędów bitowych (BER), wektora błędu modulacji (error vector magnitude, EVM), współczynnika błędu modulacji (modulation error ratio, MER) oraz efektywności energetycznej, ze szczególnym uwzględnieniem adaptacyjności w czasie rzeczywistym oraz wymagań jakości usług na poziomie systemowym (quality of service, QoS).*

Słowa kluczowe: sieci 5G, automatyczna retransmisja, stosunek sygnał-szum, inteligentne sterowanie

Introduction

The ongoing development of 5G mobile systems opens new avenues for adaptive, high-performance, and energy-sensitive communication architectures. Within the 5G framework, the physical layer – specifically, the PDSCH – plays a pivotal role [14]. This component ensures the transmission of user-centric data from the base station (gNB) to the user equipment (UE). As a pivotal element in the 5G physical layer, PDSCH significantly contributes to key network characteristics, including throughput, latency, and reliability – parameters vital for internet of things (IoT), virtual and augmented reality, smart industry, and autonomous mobility [13].

Contemporary PDSCH implementations utilize an array of cutting-edge technologies, including massive MIMO configurations, orthogonal frequency-division multiplexing (OFDM) [16], a suite of modulation formats and channel coding approaches capable of adapting to channel variations – such as low-density parity-check code (LDPC) and polar code schemes [17, 25] – as well as dynamic radio resource management. Nevertheless, even with this robust technological foundation, challenges remain in maintaining system flexibility in response to fluctuating radio channel conditions, reducing retransmission frequency, minimizing latency, and increasing resilience to transmission errors. As mobile networks grow increasingly intricate, exploring novel strategies to enhance physical-layer data transmission paths becomes highly relevant. This is particularly significant for the DL-SCH/PDSCH subsystem, which is responsible for delivering data to the end-user and serves as a prime candidate for implementing adaptive traffic control strategies, including retransmission mechanisms.

Hybrid automatic repeat request mechanisms [21], while effective in general network environments, often overlook real-time variables such as channel dynamics, modulation strategies, coding schemes, and fluctuations in user behaviour.

Against this backdrop, intelligent frameworks that employ predictive models for on-the-fly decision-making – such as determining the necessity of packet retransmission, dynamically adjusting coding parameters, or tuning modulation settings – have garnered increasing interest. Integrating HARQ with machine learning techniques, including statistical learning methods and reinforcement learning algorithms, has shown promise in boosting service quality under unpredictable radio environments.

This work introduces an intelligent processing model for the PDSCH downlink, featuring an enhanced HARQ mechanism augmented with machine learning and context-aware decision-making. The proposed approach optimizes retransmission operations by incorporating channel state insights, modulation types, coding schemes (including QC-LDPC), and overall network dynamics.

The study emphasizes the hardware implementation of the intelligent HARQ system, particularly through the use of field-programmable gate arrays (FPGAs) [5]. Due to their capacity for parallel data handling and customizable configurations, FPGAs enable low-latency operations, reduced energy consumption, and efficient execution of complex traffic management algorithms at the physical layer.

Overall, the proposed model aims to boost data exchange efficiency under volatile radio conditions, demonstrating the practical value of integrating real-time adaptive analytics with flexible 5G physical-layer mechanisms.

Below is a concise literature review highlighting key advancements in 5G physical layer development, DL-SCH/PDSCH subsystem, HARQ strategies, and the integration of intelligent control mechanisms in telecom infrastructure. Key topics include flexible encoding/modulation (QC-LDPC, polar codes, adaptive QAM), FPGA-based signal processing, and predictive channel quality optimization for retransmissions.

Article [23] discusses an enhanced HARQ method for 5G, introducing partial superposition to reduce bandwidth and power consumption. This approach improves throughput by up to 10%.

Article [3] presents a priority-based group casting HARQ method for V2V communication, increasing reliability and throughput by over 98%. Article [11] presents a radio access network orchestrator that enhances HARQ performance by 37%–88% and boosts resource utilization by 50%. Article [10] proposes a retransmission optimization for 5G NR, reducing channel usage by 15.11% by addressing dual connectivity issues. Article [1] explores power-saving enhancements in UE for 5G/B5G, with an Enhanced Paging Monitoring scheme achieving up to 37% more power savings. Article [6] introduces a multiple decoding CC-HARQ (MDCC-HARQ) scheme that improves error performance and throughput efficiency while reducing retransmissions.

In [12], channel coding challenges and solutions for 5G are reviewed, with a focus on LDPC codes under varying conditions. Article [8] evaluates LDPC performance at different signal-to-noise ratio (SNR) levels and modulation schemes like 16-QAM and 64-QAM. Article [9] discusses optimized Fast Fourier Transform (FFT) processing architectures for LTE and 5G networks, with adaptive bandwidth allocation from 10 MHz to 120 MHz.

The main contribution of this work is the design and experimental validation of an intelligent DL-SCH/PDSCH processing chain with an adaptive HARQ mechanism, integrating reinforcement learning–based decision making and subcarrier-level selective retransmission. Unlike existing HARQ enhancement approaches, the proposed framework is implemented and evaluated on an FPGA-based platform, enabling real-time adaptation based on channel quality indicators and direct comparison with a conventional baseline HARQ system.

1. Materials and methods (methodology)

The PDSCH component in 5G networks is known for its high flexibility and performance-driven architecture. It accommodates various modulation techniques, from QPSK to 1024-QAM, enabling dynamic adaptation to changing channel conditions. The use of advanced LDPC coding guarantees effective error correction, even under high data rates. Additionally, the integration of dynamic resource allocation, massive MIMO, and beamforming technologies enhances both signal quality and coverage. Efficient management of PDSCH is essential for minimizing latency, maximizing throughput, and maintaining robust performance in challenging radio environments.

Fig. 1 illustrates the structure of the DL-SCH along with the signal processing flow used for transmitting and receiving data over the PDSCH.

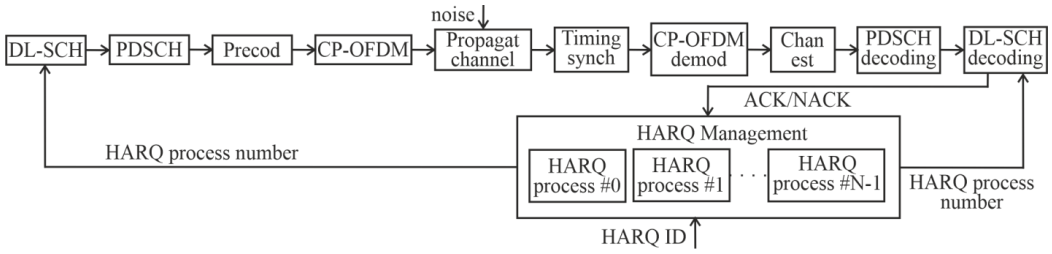

Fig. 1. Shared use DL-SCH architecture diagram

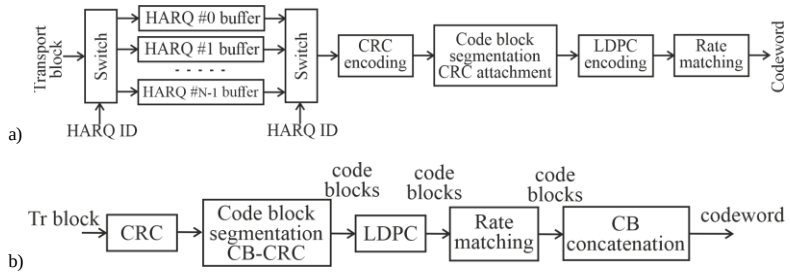

Fig. 2. Block diagram of the encoder: a) DL-SCH with HARQ processing; b) general format of the DL-SCH

At the channel level, a sequence of signal transformations is performed to enable reliable data transmission and reception within the 5G downlink. This process begins with the encoding of the DL-SCH, followed by the coordination of HARQ mechanisms to manage retransmissions. Next, the encoded data is prepared for physical layer transmission through PDSCH encoding. Multi-antenna precoding techniques, such as MIMO, are then applied to optimize spatial diversity. The signal is mapped onto subcarriers using OFDM, and subsequently passes through the propagation channel where noise and distortion may occur. On the receiving end, timing synchronization is established, OFDM demodulation is carried out, and the channel is estimated and equalized to mitigate impairments. Finally, the system performs PDSCH and DL-SCH decoding to reconstruct the original transmitted information.

The DL-SCH encoder employs internal buffers to store transport blocks for each HARQ process, selecting the content from the buffer of the active HARQ process for encoding, as depicted in Fig. 2. Similarly, the DL-SCH decoder utilizes a buffering mechanism to store and select the relevant HARQ processes for decoding. During the encoding of DL-SCH transport blocks, signal transformations occur as shown in the Fig. 2 b. In Fig. 3, we present the constructed structure of the HARQ process management block.

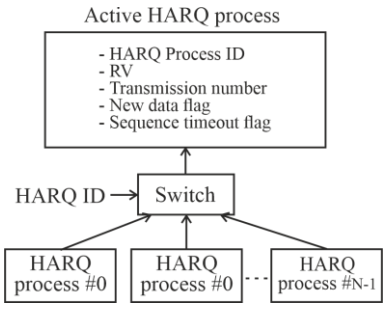

Fig. 3. Structure of the HARQ process management block

The PDSCH and demodulation reference signal (DM-RS) configuration involves selecting the modulation scheme (QPSK, 16-QAM, 64-QAM, 256-QAM, 1024-QAM), defining the resource grid (RG) dimensions (25, 52, 120, 250 RB), and setting up the DM-RS (Fig. 4). For the DL-SCH, important parameters like the coding rate, HARQ process count, and redundancy version (RV) sequences are specified, enabling retransmissions in the event of transmission failures.

The DL-SCH encoder and decoder can model up to 16 HARQ processes. The configuration of the channel outlines both the transmitting and receiving antenna count, in addition

to the signal sampling frequency used for OFDM. Transmission and reception settings include the determination of transport block size, as shown in the provided table, and the HARQ management process – in case of a transport block error, the block is retransmitted, introducing additional latency. The DL-SCH decoder buffers preserve prior codeword instances until the decoding is validated by the absence of errors, as indicated by the cyclic redundancy check (CRC) [2].

The encoded transport blocks are then converted into PDSCH symbols, followed by the application of MIMO precoding. The precoding matrix w is structured with dimensions $\nu \cdot N_{tx}$, where ν corresponds to the layer count, and N_{tx} denotes the transmit antenna configuration.

In the following, Fig. 4 depicts the structure used for encoding PDSCH symbols, while Fig. 5 shows the procedure for mapping PDSCH layers to the physical antennas of the transmitter.

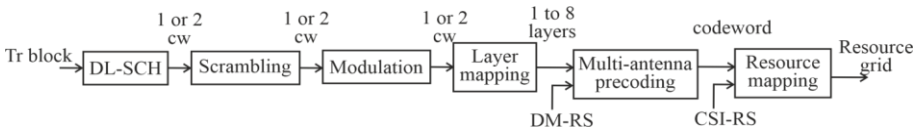

Fig. 4. Diagram of the PDSCH symbol encoding structure

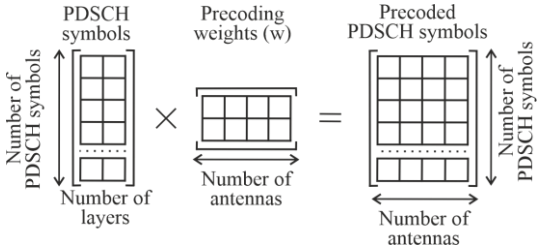

Fig. 5. Diagram illustrating the mapping of PDSCH layers to the physical antennas of the transmitter

MIMO precoding is applied to the PDSCH symbols before they are mapped to the RG. The precoded PDSCH symbols using MIMO are directed to antennas rather than layers. Fig. 6 illustrates how the MIMO precoded symbols are mapped onto the RG, with the antenna transmission configuration taken into account.

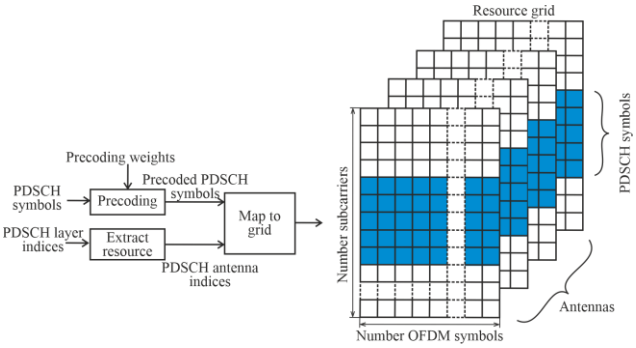

Fig. 6. The process of mapping the MIMO precoded symbols onto the RG

OFDM modulation is performed according to a predefined RG. The propagation channel processes an input of N samples and produces N output samples. However, the resulting N output samples also include a transient introduced by the channel filter, consisting of K initial samples. Since the synchronization stage removes this transient period, only $N–K$ samples remain. Unfortunately, this reduced number of samples is insufficient to decode all the data in the slot, as some of the expected slot samples are still within the delay line of the channel filter. To recover the complete set of useful output samples, the input signal is extended with a zero-padding segment. The length of this zero-padding depends on the maximum delay introduced by the channel filter. Fig. 7 illustrates the necessity of this zero-padding before the signal enters the channel. Fig. 8 presents a normalized matrix depicting correlations across the radio channel. In practical scenarios, time-domain synchronization involves correlating the received signal with reference DM-RS symbols transmitted over the PDSCH. Following synchronization, OFDM demodulation is carried out. Channel estimation enables the mapping of propagation effects onto individual resource elements (REs). This estimated information is then utilized by the equalizer to counteract channel-induced distortions. In Fig. 9, the multipath structure of the channel is illustrated via its impulse response (CIR). Practical channel estimation captures the propagation environment between spatial layers and receiving elements. This process also incorporates the influence of MIMO precoding (Fig. 10).

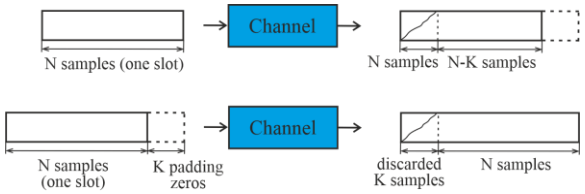

Fig. 7. Transformation of the PDSCH samples prior to transmission through the communication channel

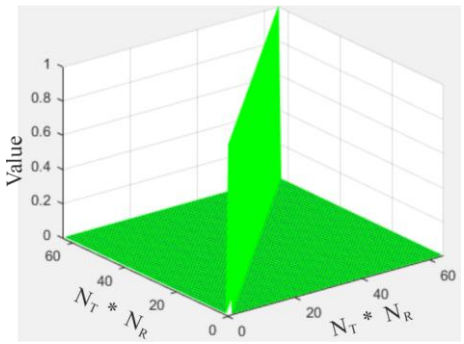

Fig. 8. Normalized matrix representing spatial signal similarity: N_T – count of sending elements; N_R – count of receiving elements

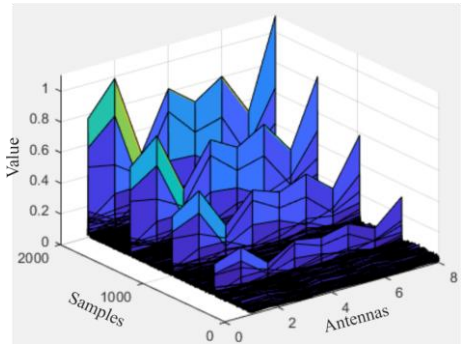

Fig. 9. Simulated CIR for an eight-antenna configuration

An illustration in Fig. 10 depicts the positioning of reference elements for channel estimation as part of the downlink processing pipeline.

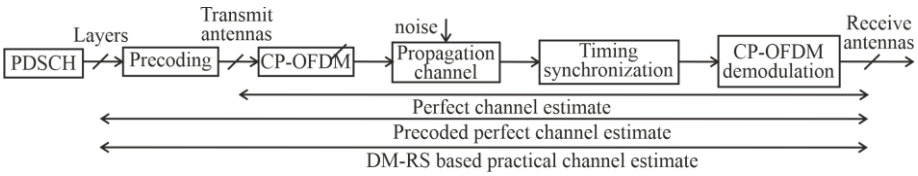

Fig. 10. Illustration showing the positioning of reference elements for channel estimation

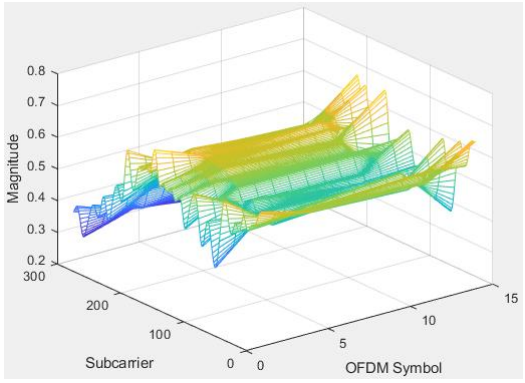

Fig. 11. Channel estimation (SNR = 20 dB) between the first layer and the first receive antenna

In Fig. 11, the channel estimation (SNR=20 dB) is shown for the link between layer one and the first receiving antenna.

At subsequent stages of signal processing, the equalizer utilizes the channel estimation to mitigate distortions. The PDSCH symbols are retrieved from the received grid together with the corresponding channel estimates. The variable channel state information (CSI) contains the channel state information for each symbol. CSI is used to align the PDSCH symbols. The CSI signal is depicted in Fig. 12.

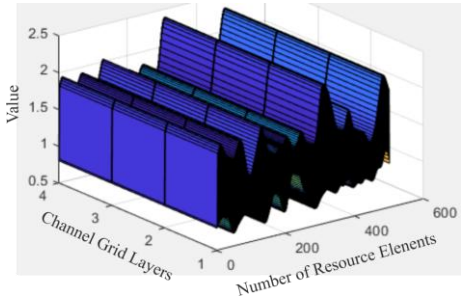

Fig. 12. Graphical representation of the signal illustrating CSI

Following this, the aligned PDSCH symbols are decoded to retrieve the soft-bit code word. Next, the soft bits, or logarithmic likelihood ratios (LLR) [7], are scaled according to the CSI. This scaling method gives more weight to the RE that experience more favorable channel conditions. Following this, the DL-SCH decoding procedure occurs, where the LLR values are processed, and the transport block is examined for potential errors.

Finally, the current HARQ process is updated with the block error status, and the system proceeds to the next process. This step refreshes the data linked to the ongoing HARQ process.

We now turn our attention to the configuration of the downlink frame in 5G, where communication from the base station to the UE is structured to support multiple antenna ports. These ports serve as logical paths for transmitting data, enabling enhanced reliability through transmit diversity or increased throughput via spatial multiplexing.

Fig. 13 illustrates the concept of the 5G resource structure, including RG, resource blocks, and REs.

In Fig. 14, the connection between antenna interfaces and physical antenna elements is illustrated. A single antenna port may correspond to either a single physical antenna or a group of them.

Both the physical PDSCH and its associated DM-RS utilize the same antenna port. This setup allows the UE to estimate the propagation channel using DM-RS and apply that knowledge to decode the data carried by the PDSCH.

As shown in Fig. 15, the MIMO framework leverages multiple antenna ports to transmit several parallel data streams. Consequently, the modulated data symbols can be routed to one or more physical antennas depending on the spatial processing strategy.

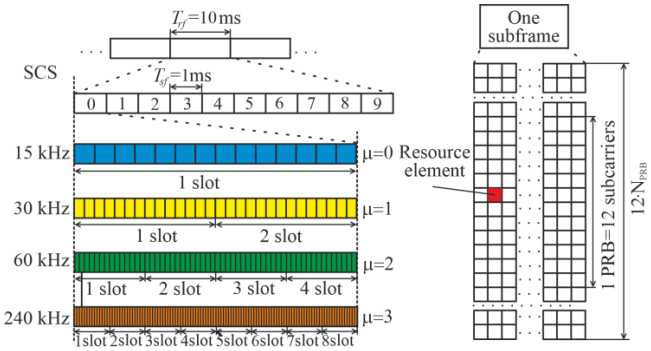

Fig. 13. The concept of the 5G resource structure

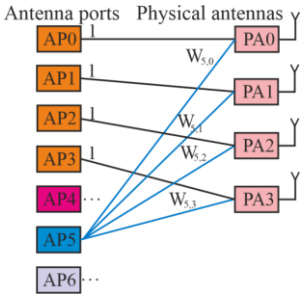

Fig. 14. Mapping of logical antenna interfaces to physical antenna hardware structure

Fig. 15 presents the configuration of signal connections directing the signals to the physical antenna.

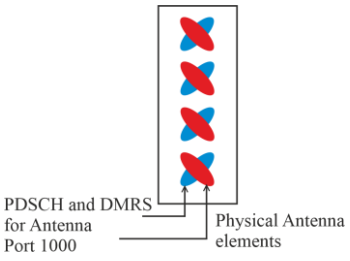

Fig. 15. The setup of signal connections directed to the antenna hardware

In Fig. 16, the modulated symbols from all transmission layers are first aggregated and then redistributed across the available antenna ports before entering the precoding stage. After precoding is applied, each resulting symbol is mapped to specific resource elements, with the mapping process handled individually for each antenna port. Independent RG are created for each antenna port prior to the inverse FFT (IFFT), which is part of OFDM signal generation [18].

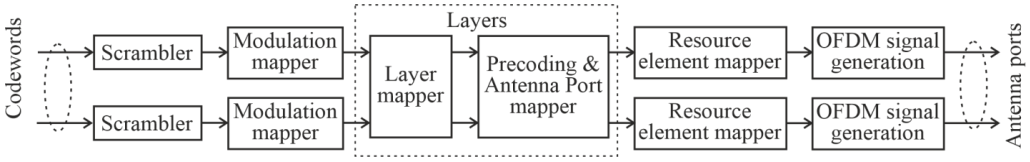

Fig. 16. Structure of the signal conversion pathway for codeword transmission and its link to the physical antenna interface

2. Results

We describe the transformations in the PDSCH scheme (Fig. 1) through the following equations:

$$\mathbf{b}_{HARQ}^{(t)} = \begin{cases} \mathbf{b}, & t=0 \\ \mathbf{b} \otimes \mathbf{b}_{HARQ}^{(t-1)}, & t>0 \end{cases} \tag{1}$$

$$\mathbf{c} = \varepsilon(\mathbf{b}_{HARQ}^{(t)}) \tag{2}$$

$$x_k = M(c_{km}, ..., c_{(k+1)m-1}), k = 0, ..., N_s - 1 \tag{3}$$

$$\mathbf{x} = \left[x_0, ..., x_{N_s-1} \right]^T \tag{4}$$

$$\mathbf{x}_{MIMO} = \mathbf{W} \times \mathbf{x} \tag{5}$$

$$\mathbf{s} = F_N^{-1}(\mathbf{x}_{MIMO}) \tag{6}$$

$$\mathbf{s}_{CP} = C_{CP}(\mathbf{s}) \tag{7}$$

$$y_i(t) = \Re\left\{ s_{CP,i}(t) \cdot e^{j2\pi f_c t} \right\}, i = 1, ..., N_t \tag{8}$$

where in (1)–(8) we used a set of symbolic notations to represent the signal at different stages of the PDSCH processing chain, each reflecting a specific transformation or physical form of the data. Specifically, $\mathbf{b} \in \{0,1\}^K$ denotes the data block from the DL-SCH; $\mathbf{b}_{HARQ}$ represents the result of HARQ combining; $\mathbf{c} \in \{0,1\}^{N_c}$ refers to the bitstream after LDPC encoding; $\mathbf{x} \in \mathbb{C}^{N_s}$ stands for the QAM symbols; $\mathbf{x}_{MIMO} \in \mathbb{C}^{N_t}$ captures the signal prepared for transmission through the antennas; $\mathbf{s} \in \mathbb{C}^N$ reflects the OFDM symbols prior to cyclic prefix (CP) insertion; $\mathbf{s}_{CP} \in \mathbb{C}^{N+N_{CP}}$ is the OFDM signal with the CP included; the matrix $\mathbf{W}$, functioning as a precoder, is generally applied to the *k*-th subcarrier – further details follow and $y(t) \in \mathbb{R}^{N_t}$ is the final time-domain waveform ready for over-the-air transmission. For notation purposes, we assign N_t to represent the number of transmit antennas, N_s to indicate the number of data streams, and N_{SC} to denote the total subcarrier count.

Rather than treating these stages as isolated black boxes, we interpret them as a continuous signal evolution process. The chain begins with HARQ combining (1), a crucial step that integrates information from multiple transmission attempts to reinforce decoding confidence. This is followed by LDPC encoding (2), which introduces structured redundancy for forward error correction [2]. (3) marks the transition into the modulation domain, mapping the encoded bits into QAM symbols – a necessary step for preparing data for physical-layer transmission. The symbol vector itself is explicitly represented in (4), serving as a bridge to spatial domain processing. In (5), the application of MIMO precoding adjusts the transmission according to the antenna arrangement and the characteristics of the channel. Transitioning from frequency to time domain is performed via IFFT, as outlined in (6), which marks the beginning of the OFDM modulation process. Prior to transmission, a CP is added as shown in (7), reducing the impact of delay spread and maintaining symbol orthogonality. The final transformation (8) takes the baseband OFDM signal and shifts it into the RF domain, producing the real-valued waveform *y*(*t*) that propagates through the wireless channel.

Building on the description provided above, we present a detailed mathematical formulation of the transformations, explicitly highlighting the applied operations. After the MIMO precoding stage, the symbols x_k are transmitted in sequence and converted into several parallel data paths. Every path is associated with a particular transmitting antenna and occupies separate resource units within the time-frequency grid (RB) of the OFDM system. The distribution scheme involving RBs is outlined below:

$$x_k^{(a)} \rightarrow X_{r,t}^{(a)} \in \mathbb{C} \tag{9}$$

where $a \in \{1, ..., N_t\}$ is the MIMO steam index; $r \in \{0, ..., R-1\}$ is the RB-index; $t \in \{0, ..., T-1\}$ is the index of the OFDM symbol in the time domain.

This illustrates how the data sequence is allocated to a two-dimensional RG (Fig. 5, 6, and 13). Following the transformation into the frequency domain, we introduce a mathematical representation of how the vector of frequency components is constructed for each time instant *t*.

$$\mathbf{X}_t^{(a)} = \left[X_{0,t}^{(a)}, X_{1,t}^{(a)}, ..., X_{N_{sc}-1,t}^{(a)} \right] \tag{10}$$

The vector formed in equation (10) is then processed through the IFFT.

$$\mathbf{x}_t^{(a)} = F_N^{-1}(\mathbf{X}_t^{(a)}) = \frac{1}{\sqrt{N_{sc}}} \sum_{n=0}^{N_{sc}-1} X_{n,t}^{(a)} e^{j2\pi \frac{kn}{N_{sc}}} \tag{11}$$

where $k \in \{0, ..., N_{sc}-1\}$.

We generate a CP of length L_{CP} for every OFDM symbol, enabling its subsequent over-the-air transmission from the antenna.

$$s_t^{(a)} = [x_t^{(a)}[N_{sc} - L_{CP}], ..., x_t^{(a)}[N_{sc}-1], x_t^{(a)}[0], ..., x_t^{(a)}[N_{sc}-1]] \tag{12}$$

We also place emphasis on HARQ alongside the encoding and scrambling processes. We represent the unfolded bit sequence from equation (1) in the following form:

$$\mathbf{b} = \left[b_0, b_1, ..., b_{K-1} \right] \in \mathbb{Z}_2^K \tag{13}$$

Following the encoding stage – where we specifically focus on the LDPC scheme – the resulting structure is unfolded as follows:

$$\mathbf{c} = \mathrm{LDPC}_R(\mathbf{b}) \in \mathbb{Z}_2^N \tag{14}$$

Here, $R = K / N$ denotes the coding rate as defined in our notation. Ultimately, the coding scheme is merged with HARQ functionality by means of splitting into code blocks and allowing retransmissions via IR-HARQ.

$$\mathbf{c}^{(i)} = \mathrm{HARQ}_{IR}(c, i), i = 1, 2, ... \tag{15}$$

In the context of HARQ, we also take scrambling into account, where the scrambling sequence s_n is generated based on parameters such as the cell identifier, slot number, and the HARQ process index.

$$\tilde{c}_n = c_n \otimes s_n \tag{16}$$

Consequently, a pseudorandom sequence is employed in the process. In the experimental section of the paper, we employ *M*-QAM signals (with *M* = 16,64,256), accordingly, the symbols are mathematically constructed by grouping the scrambled bits from equation (16) as follows:

$$x_k = \mathrm{Mod}_M(\tilde{c}_{k\cdot\log_2 M},...,\tilde{c}_{(k+1)\cdot\log_2 M-1}) \in \mathbb{C} \quad (17)$$

Based on (5), we proceed with re-encoding and perform OFDM modulation as described in (11). This is followed by the introduction of an intelligent HARQ scheme. The core idea lies in applying an adaptive mechanism in which the retransmission threshold dynamically adjusts according to current channel conditions and quality of service (QoS) requirements. Traditionally, HARQ systems rely on a fixed threshold to determine the need for retransmission [21]. In contrast, we leverage the phase states of the channel and error statistics to guide the system in optimizing the retransmission timing. As will be demonstrated later in the paper, this approach effectively balances throughput and reliability.

A mathematical representation of the adaptive threshold HARQ is introduced as follows:

$$\chi(t) = \chi_{\min} + \delta\chi(t) \quad (18)$$

where $\chi(t)$ is the dynamically adjusted error threshold at step *t*; $\chi_{\min}$ indicates its lower bound; $\delta\chi(t)$ models its variation with respect to the channel condition.

Leveraging the combination of MIMO and OFDM [4, 20, 22, 24], we propose a retransmission strategy that functions independently for each active subcarrier, informed by localized channel state analysis. When a particular subcarrier exhibits degraded quality, the system selectively initiates a retransmission request – targeting only the affected subcarriers. This approach preserves the overall throughput across the remaining subcarriers, ensuring more efficient resource utilization.

The mathematical formulation of this process is expressed as:

$$P_{r,n}(t) = \frac{1}{1+\exp(-\chi_n(t))} \cdot P_{r,b}(t) \quad (19)$$

As the channel quality indicator $\chi_n(t)$, we used the SNR for the *n*-th subcarrier at time *t*. Thus, in (19), $P_{r,n}(t)$ represents the resulting probability of retransmission, while $P_{r,b}(t)$ denotes the baseline retransmission probability, set globally or according to QoS requirements.

The use of $\exp(x)$ is chosen for its properties of continuity and differentiability, making it well-suited for optimization tasks and simulations, which are crucial for the experiments presented later in this paper. From the perspective of AI implementation, gradient analysis, machine learning, and adaptive systems benefit from this approach. The function acts as a 'threshold smoother', ensuring a smooth transition in the channel's uncertainty zone, rather than relying on abrupt decision-making. This approach significantly optimizes the complex system when forming RB and applying the HARQ mechanism.

The functioning of the suggested intelligent HARQ system proceeds as follows: 1) Initially, the channel is assessed. At each transmission stage, the system analyzes the channels for each subcarrier and spatial zone using MIMO and the RG. 2) On the second step, the adaptive threshold is configured. For each symbol, the error threshold is modified according to the anticipated channel state. 3) In the third stage, a retransmission request is generated. If the error exceeds the adaptive threshold, retransmission is requested only for those parts that require improvement. 4) Finally, the fourth stage involves intelligent correction. By applying machine learning (ML) methods, the system predicts the need for retransmission requests based on the incoming data about the channel conditions.

To clarify the distinctive feature of the decision-making process in the system, we enhance formula (18) with a mathematical model for integrating the intelligent HARQ system. Thus, we define the context of the predicted probability of a retransmission request as follows:

$$P_r(t) = V_{ML}(C_{ch}(t), P_{r,b}(t)) \quad (20)$$

where V_{ML} is the ML model that predicts the need for retransmission requests based on the channel assessment $C_{ch}(t)$.

To provide more details on this $C_{ch}(t)$, we present the mathematical model for channel state estimation, including the parameters discussed earlier, particularly the applied modulation and coding scheme. For AI or ML-based channel estimation, we construct a model that, based on historical data and current values of received signal strength indicator (RSSI), SNR, as well as encryption and modulation coefficients, predicts the likelihood of the need for a HARQ retransmission request.

$$C_{ch}(t) = V_{ML}(\mathrm{RSSI}(t), \mathrm{SNR}(t), \mathrm{Mod}(t), \mathrm{Cod}(t)) \quad (21)$$

The result we obtain is that the model can be trained on historical communication channel data collected in real time. This allows the system to account for variations in the communication channel and adapt the HARQ system to different conditions. The threshold in (19) can be time-varying, depending on changes in SNR, bit error rates, and other factors that affect transmission reliability. The intelligent system can use an optimization algorithm (for instance, we explored gradient descent) to find the most effective threshold in real time. Additionally, we anticipate that the algorithm can account for dynamic channel changes and adjust the threshold for each stage. As a result, we observe a reduction in unnecessary retransmission requests for frequencies with favorable channel conditions, thereby improving resource utilization efficiency. To formalize this optimization approach, we propose the concept of using reinforcement learning (RL) for adaptive retransmission control, where ML agents learn (AL) optimal retransmission strategies based on past experience and the current channel state. Thus, the AL model for HARQ is presented as follows:

$$Q(s,a) = \max(R(s,a) + \gamma \cdot \max_{a'} Q(s',a')) \quad (22)$$

where $Q(s,a)$ is the quality function for state *s* and action *a*; $R(s,a)$ is the reward for performing action *a* in state *s*; γ is the discount factor; a' – future action in the new state - s'.

This part of the article outlines the outcomes of experimental research conducted using a Simulink-based model of the 5G PDSCH. The theoretical background and practical implementation details of the model were discussed in the preceding section.

For the experimental setup, the FPGA AXU2CGB development board – featuring the Xilinx XCZU2CG chip (Fig. 17) and integrated with Matlab – was employed. The synthesized Simulink representation of the 5G PDSCH developed for this study is illustrated in Fig. 18.

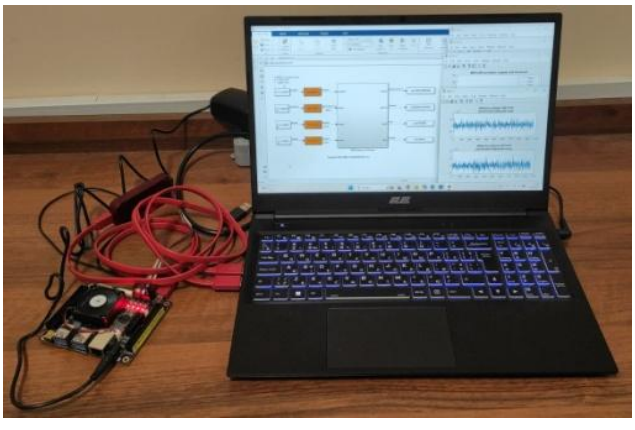

Fig. 17. Test bench arrangement with AXU2CGB evaluation platform

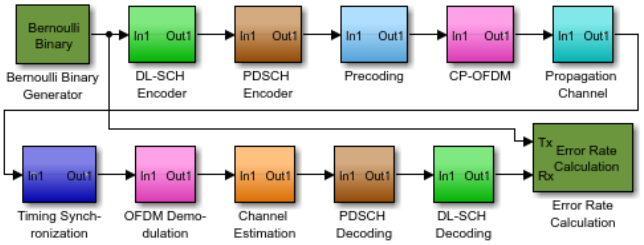

Fig. 18. DL-SCH simulated in Simulink

To initialize the developed model, a set of baseline parameters was defined to ensure flexibility in the simulation environment. The FFT size was varied from 512 to 4096, which corresponded to bandwidth values ranging between 10 MHz and 120 MHz. The structure of the RG was adapted accordingly, with the number of physical RBs ranging from 25 to 250 (Fig. 13). The transport block, generated as a result of modulation synthesis using *M*-QAM schemes, varied in size from 5,760 to 57,376 bits. Conditions for OFDM symbol generation were established by modifying the subcarrier spacing (between 15 and 60 kHz) and adjusting the CP duration from 4.7 µs to 1.2 µs. Coding rates were determined through the use of LDPC-based error correction techniques, decoded via the normalized min-sum algorithm [17]. Moreover, the model allowed for dynamic adjustment of transmission structure settings, such as the number of symbols in each slot, the slots per subframes, and the total number of slots per frame (ranging from 10 to 40), along with the system's sampling rate.

To assess the impact of various parameters on channel quality and model training, we conducted an analysis of several key indicators that directly influence the performance and efficiency of the system under real operational conditions. During the study, the error vector magnitude (EVM) was assessed using (23), quantifying how much the received symbol deviates from its optimal position in the modulation constellation of the signal. Additionally, the modulation error ratio (MER) was used as a metric to gauge the presence of noise (SNR) in the modulated signal, with its value calculated in decibels [24]. This evaluation was performed for a data packet containing *N*-symbols, as specified in (24). Moreover, the bit error rate (BER) was calculated according to (25). These assessments play a vital role in optimizing 5G modulation techniques [15] to improve data integrity and transmission efficiency, facilitating the identification of robust configurations that meet the requirements of contemporary wireless communication systems.

$$EVM_{RMS} = \sqrt{\frac{\frac{1}{N}\sum_{k=1}^{N}(e_k)}{\frac{1}{N}\sum_{k=1}^{N}(I_k^2+Q_k^2)}}\cdot 100 \tag{23}$$

$$MER_{dB} = 10\cdot\log\left(\frac{\sum_{k=1}^{N}\left(I_k^2+Q_k^2\right)}{\sum_{k=1}^{N}e_k}\right) \tag{24}$$

$$BER \approx \frac{4}{\log_2(M)}\cdot Q\left(\sqrt{\frac{3\cdot SNR}{M-1}}\right) \tag{25}$$

where in the above expressions, the following notations are applied: $e_k = \left(I_k - \tilde{I}_k\right)^2 + \left(Q_k - \tilde{Q}_k\right)^2$; I_k denote the ideal in-phase value of the *k*-th symbol within the packet; Q_k corresponds to the ideal quadrature component of the same symbol; $\tilde{I}_k$ and $\tilde{Q}_k$ represent the actual in-phase and quadrature components as determined by the receiver; N indicates the total number of symbols included in the analysed packet; M refers to the modulation order; SNR stands for the signal-to-noise ratio; $Q(x) = \frac{1}{\sqrt{2\pi}}\int_x^{\infty} e^{-t^2/2}dt$ denotes the error integral used in the evaluation process.

In soft decision mode, the demodulator generates an output where the log-likelihood ratios (LLRs) of the demodulated bits include both positive and negative values, as shown in Fig. 19. The signal output from the demodulator in soft decision mode includes both positive and negative LLR values for the decoded bits, as shown in Fig. 19. Positive LLRs suggest a higher likelihood of the bit being '1', whereas negative values imply a greater chance of the bit being '0'. This representation retains valuable uncertainty information, which plays a vital role in decoding algorithms such as LDPC [4].

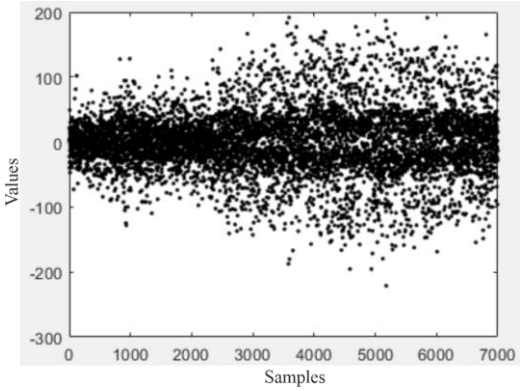

Fig. 19. Visualization of LLRs for decoded bits

A 2048-point FFT was computed on the DL-SCH signal, and the resulting spectrum is illustrated in Fig. 20.

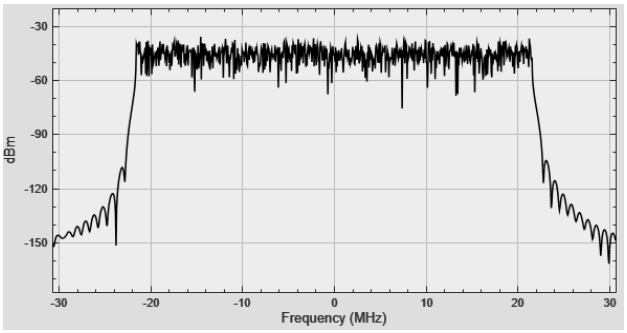

Fig. 20. DL-SCH signal spectrum obtained via 2048-point FFT analysis

In Fig. 21, the EVM versus SNR performance for PDSCH is shown for different modulation formats with a 2048-point FFT configuration.

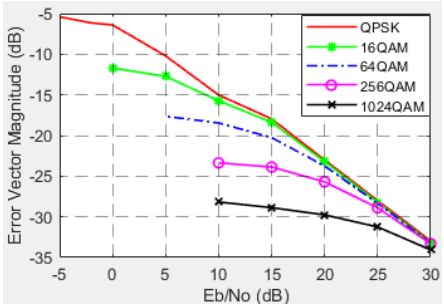

Fig. 21. EVM versus SNR curves for PDSCH under various modulation schemes using a 2048-point FFT

When the EVM is high, the received symbols may cross decision boundaries within the constellation diagram, increasing the likelihood of bit errors. Conversely, a low EVM indicates minimal deviation from ideal symbol positions, which helps maintain a low BER.

Fig. 22 illustrates how MER varies with SNR for the PDSCH signal across several modulation schemes, using a 2048-point FFT.

We conducted the study using a mathematical model for the MER, represented by (23).

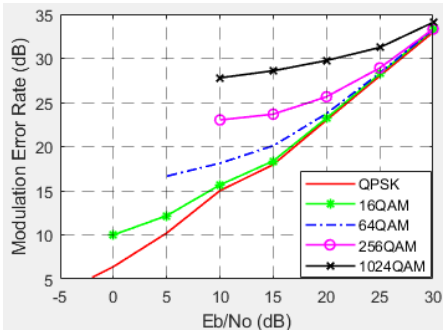

Fig. 22. MER versus SNR performance for PDSCH with various modulation schemes and a 2048-point FFT

Fig. 23 illustrates the relationship between BER and SNR for the PDSCH, considering multiple modulation formats and a 2048-point FFT.

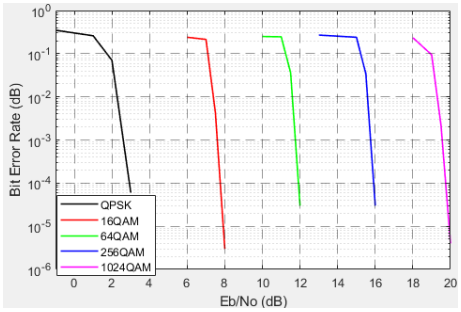

Fig. 23. BER versus SNR graph for the PDSCH with various modulation schemes and a 2048-point FFT

Fig. 24 presents the relationship between throughput and SNR for the PDSCH, evaluated with different modulation schemes and a 2048-point FFT.

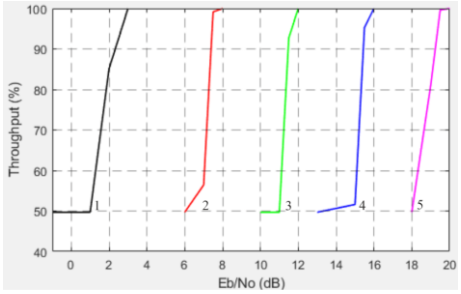

Fig. 24. Throughput versus SNR graph for the PDSCH with various modulation schemes and a 2048-point FFT: 1 is the QPSK; 2 is the 16-QAM; 3 is the 64-QAM; 4 is the 256-QAM; 5 is the 1024-QAM

The graph in Fig. 25 illustrates how the BER correlates with the EVM for the PDSCH, using various modulation schemes and a 2048-point FFT.

Analysis of the presented graphs reveals that QPSK modulation exhibits the greatest energy efficiency, transmitting 2 bits/symbol. As the modulation order increases by 2 bits/symbol, a corresponding decrease in energy efficiency of approximately 2 dB is observed. To maintain the EVM within the standard-defined limits, the values are as follows: QPSK – -15.14 dB; 16-QAM – -18.062 dB; 64-QAM – -21.94 dB; 256-QAM – -29.12 dB; 1024-QAM – -35 dB.

The EVM and BER are interrelated, as EVM characterizes the quality of the received signal, while BER determines the likelihood of bit errors during decoding. Higher EVM values correspond to a greater probability of bit errors, meaning that the BER increases as well. EVM represents the average deviation of the received symbols from their ideal positions in the modulation constellation. BER depends on how significantly these deviations lead to erroneous demodulation.

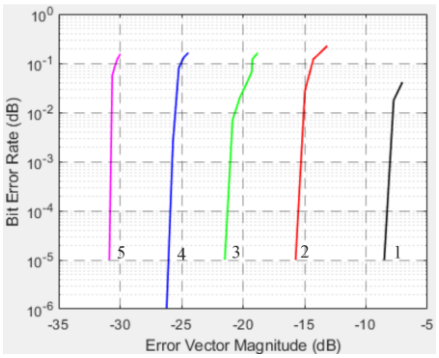

Fig. 25. BER versus EVM graph for the PDSCH with various modulation schemes and a 2048-point FFT: 1 is the QPSK; 2 is the 16-QAM; 3 is the 64-QAM; 4 is the 256-QAM; 5 is the 1024-QAM

When the EVM is high, symbols may cross decision region boundaries in the constellation (Fig. 26), leading to bit errors. Conversely, when the EVM is low, the deviations are minimal, and the BER remains low.

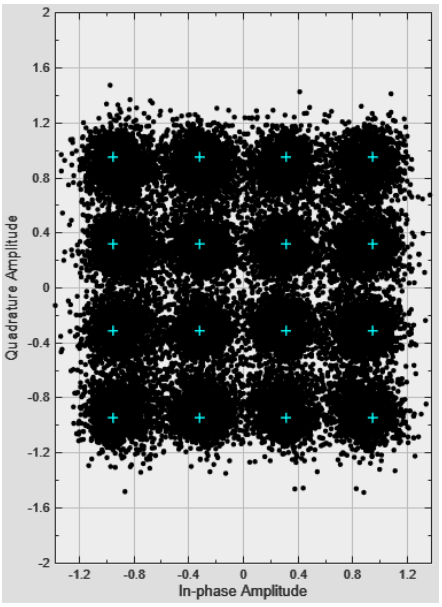

Fig. 26 Signal constellation for 16-QAM modulation (EVM – 17.86% (-14.96 dB), MER – 14.85 dB, SNR – 8 dB, BER – 0.0275)

The evaluation of EVM, MER, and BER values based on the assessed SNR values was employed for training a neural network, with a specific focus on validating the proposed intelligent HARQ. In other words, we prepared the input data for the AI network. Therefore, these indicators served as quality metrics that assist the network in adapting demodulation and HARQ strategies according to the actual channel conditions. Additionally, through the RL strategy described in (21), we developed a concept for applying this algorithm in situations where the system adjusts its signal processing strategies based on EVM, MER, and BER values derived from the assessed SNR, which enhances demodulation accuracy and HARQ analysis. The application of the RL concept, in general, facilitates training aimed at adjusting threshold values for constellation point recognition depending on the signal state, thus reducing classification errors.

To assess the efficiency of implementing an intelligent HARQ system, we conducted an evaluation based on several core performance indicators. These metrics included throughput (representing the average bit rate achieved per time unit), latency (reflecting the delay in packet delivery, accounting for retransmission delays within the HARQ processes), power efficiency (indicating the energy required to sustain a specified performance level or BER), and the BER, analyzed as a function of different SNR levels.

The experiment focused on analyzing HARQ throughput in a 5G context, with SNR values ranging from 0 to 20 dB. A synthetic dataset was used to simulate realistic channel conditions across this range, reflecting common reception scenarios in next-generation wireless networks. For the intelligent HARQ model, RL was employed to enable dynamic adjustment of retransmission thresholds in response to real-time channel conditions. In contrast, the baseline traditional HARQ used fixed thresholds. The adaptive model was trained using channel quality metrics such as EVM, MER, BER, and SNR, obtained from preliminary simulations (refer to Fig. 21–26). A throughput cap of 100 Mbps was defined to represent high-bandwidth use cases such as video streaming or smart city communications. Both HARQ strategies – traditional and intelligent – were modelled and compared to evaluate the potential gains from integrating ML into retransmission logic (Fig. 27).

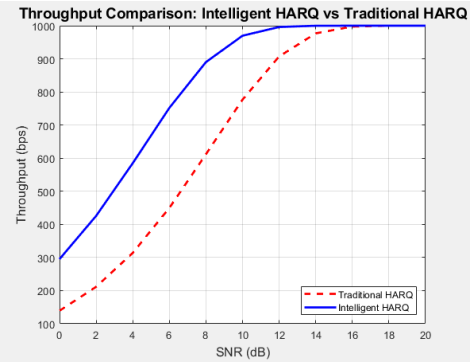

Fig. 27. Throughput comparison: intelligent HARQ vs traditional HARQ

Based on the experimental findings, it is evident that the intelligent HARQ system demonstrates a substantial performance improvement over the traditional approach, especially under low and moderate SNR conditions. For instance, at SNR=10dB, the traditional HARQ achieves a normalized throughput of approximately 0.79, while the intelligent HARQ reaches 0.98, representing a 24% improvement. Similarly, at SNR=5dB, throughput increases from 0.40 (traditional) to 0.69 (intelligent), yielding a 72.5% gain. At high SNR values (e.g., 20 dB), both systems approach maximum throughput levels. However, the intelligent HARQ converges faster, requiring fewer retransmissions and exhibiting reduced latency. This efficiency stems from the system's capacity to leverage past channel data and adjust retransmission thresholds in response.

Overall, the intelligent HARQ demonstrates a performance boost of 25–70% across the low-to-mid SNR range – an advantage that is especially critical in mobile environments with fluctuating signal conditions. These gains directly translate to improved quality of service in real-world applications, including lower latency in video streaming, enhanced connection stability in online gaming and XR/VR experiences, reliable communication for autonomous vehicles and IoT devices, as well as more efficient utilization of radio spectrum and energy resources, which is essential for next-generation mobile networks.

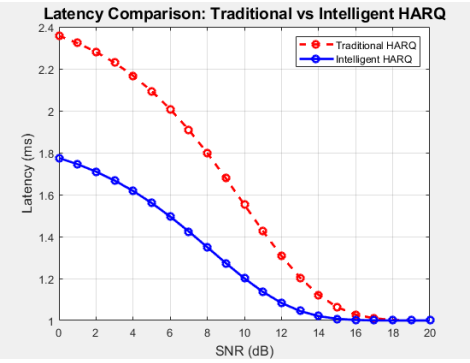

Fig. 28. Latency vs SNR for traditional and intelligent HARQ

Fig. 28 illustrates the latency performance across different SNR values for traditional and intelligent HARQ.

A comparative analysis of traditional and intelligent HARQ procedures at an SNR of 10 dB revealed that the proposed intelligent approach reduces packet delivery latency from 1.57 ms to 1.21 ms, representing a reduction of approximately 22.8%. This improvement is primarily due to a significant decrease in BER, from 0.184 to 0.0669 – an enhancement of over 2.7 times. Additionally, signal quality is improved, with EVM reduced from 31.6% to 25.3%, and MER increased from 10.0 dB to 12.0 dB. Such latency reduction is critical for ultra time-sensitive 5G applications, particularly in domains like autonomous transportation (V2X), where decisions must be made in under a millisecond, as well as remote surgery, cloud gaming, augmented and virtual reality (AR/VR), where ultra-low latency is essential for proper interaction. Furthermore, these gains are vital for Industry 4.0 environments, which demand precise synchronization between sensors and robotic systems.

Fig. 29 presents a comparison of HARQ schemes in terms of power efficiency, quantified as the energy needed to maintain a particular performance level or BER.

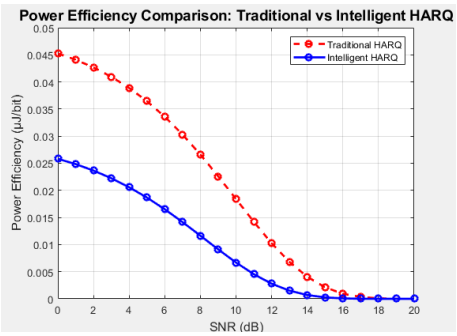

Fig. 29. Power efficiency comparison of traditional and intelligent HARQ systems

The intelligent HARQ system demonstrates significantly higher energy efficiency compared to its traditional counterpart. At a SNR of 10 dB, the intelligent system consumes ≈ 0.010 µJ/bit, which is about 44% more efficient compared to the traditional HARQ system, which consumes 0.018 µJ/bit. This enhancement results from a reduction in BER and the optimization of the retransmission process, enabling the system to sustain high throughput while minimizing energy consumption. Such energy savings are especially critical in 5G applications like V2X, where lowering power consumption ensures continuous operation of communication modules. In remote surgery and AR/VR systems, both low latency and energy efficiency are essential for stable interaction. Similarly, in Industry 4.0 environments, reduced energy demands enable prolonged autonomous operation of robotic systems and sensor networks.

3. Discussion and conclusion

The results of this study demonstrate a significant performance improvement of the proposed intelligent HARQ system in 5G, particularly in the low-to-moderate SNR range (5–10 dB). Throughput gains of 30–70% were achieved, alongside reduced latency and enhanced energy efficiency compared to traditional HARQ. These improvements are particularly crucial for 5G applications with stringent latency and reliability requirements, such as V2X, remote surgery, and augmented/virtual reality. The intelligent HARQ system, driven by ML, is capable of dynamically adjusting retransmission control, optimizing throughput while minimizing power consumption.

From a comparative perspective, the obtained results indicate that the proposed intelligent HARQ framework outperforms conventional and recently reported HARQ enhancement schemes particularly under low-to-moderate SNR conditions, where static retransmission strategies are inherently inefficient.

Unlike existing approaches that focus on protocol-level or fixed-parameter optimizations, the observed gains stem from joint learning-driven decision making, subcarrier-level selectivity, and real-time hardware-aware adaptation, which collectively explain the performance advantages demonstrated in the results section.

However, the results highlight that the observed improvements represent the upper-bound potential, especially in conditions where traditional HARQ is suboptimal. In real-world networks, performance may vary due to channel fluctuations, limited training data, and computational constraints, with improvements ranging between 20–50%. The effectiveness of the intelligent HARQ system is heavily dependent on the RL agent's training – requiring a diverse training dataset, a well-balanced reward function across throughput, latency, and energy efficiency, and real-time adaptability to channel metrics such as EVM, MER, SNR, and BER while adhering to QoS requirements and system resource limitations. The findings support the viability of intelligent HARQ for next-generation 5G and future 6G networks, contributing to the development of adaptive and efficient communication systems.

This work provides a novel end-to-end intelligent HARQ framework that combines reinforcement learning–based retransmission control with subcarrier-level selectivity and FPGA-based real-time validation within the DL-SCH/PDSCH chain.

By bridging algorithmic design, hardware implementation, and system-level performance evaluation, the proposed approach clearly distinguishes itself from existing HARQ optimization methods and establishes a practical pathway toward adaptive physical-layer control in 5G and beyond.

Future research can explore extending the proposed intelligent HARQ framework to multi-cell and massive MIMO scenarios, as well as incorporating more advanced reinforcement learning strategies for dynamic spectrum allocation. Additionally, investigating real-world deployment and interoperability with emerging 6G physical-layer technologies will further validate and enhance the adaptability of the system.

References

[1] Agiwal, A., & Agiwal, M. (2022). Enhanced Paging Monitoring for 5G and Beyond 5G Networks. *IEEE Access*, *10*, 27197–27210. https://doi.org/10.1109/ACCESS.2022.3157874

[2] Alphiya, A., & Latha, T. (2025). An Efficient QC-LDPC channel encoder/decoder architecture with parallel vector-matrix computations for 5G wireless networks on FPGA. *Computer Networks*, *264*, 111229. https://doi.org/10.1016/j.comnet.2025.111229

[3] An, S., & Chang, K. (2023). Enhancing Reliability in 5G NR V2V Communications Through Priority-Based Groupcasting and IR-HARQ. *IEEE Access*, *11*, 72717–72731. https://doi.org/10.1109/ACCESS.2023.3292150

[4] Boiko, J., Pyatin, I., & Eromenko, O. (2022). Analysis of Signal Synchronization Conditions in 5G Mobile Information Technologies. *2022 IEEE 16th International Conference on Advanced Trends in Radioelectronics, Telecommunications and Computer Engineering (TCSET)*, 01–06. https://doi.org/10.1109/TCSET55632.2022.9766899

[5] Borromeo, J. C., Kondepu, K., Andriolli, N., & Valcarenghi, L. (2022). FPGA-accelerated SmartNIC for supporting 5G virtualized Radio Access Network. *Computer Networks*, *210*, 108931. https://doi.org/10.1016/j.comnet.2022.108931

[6] Chen, H., Liao, L., Li, C., Liu, Y., Sun, Y., & Li, X. (2023). Multiple decoding for polar-coded chase combining HARQ. *Physical Communication*, *56*, 101955. https://doi.org/10.1016/j.phycom.2022.101955

[7] Hu, Z., Chen, F., Wen, M., Ji, F., & Yu, H. (2018). Low-Complexity LLR Calculation for OFDM With Index Modulation. *IEEE Wireless Communications Letters*, *7*(4), 618–621. https://doi.org/10.1109/LWC.2018.2802949

[8] Indoonundon, M., & Pawan Fowdur, T. (2021). Overview of the challenges and solutions for 5G channel coding schemes. *Journal of Information and Telecommunication*, *5*(4), 460–483. https://doi.org/10.1080/24751839.2021.1954752

[9] Khan, D., Jan, L., & Zafar, M. H. (2025). Optimized FFT Designs for High-Performance LTE and 5G Networks. *Arabian Journal for Science and Engineering*, *50*(21), 17555–17574. https://doi.org/10.1007/s13369-025-10009-z

[10] Lee, C., Kim, J., Jung, J., Baik, J., & Chung, J.-M. (2022). HARQ Optimization for PDCP Duplication-Based 5G URLLC Dual Connectivity. *Computers, Materials & Continua*, *72*(1), 727–738. https://doi.org/10.32604/cmc.2022.024824

[11] Maule, M., Vardakas, J. S., & Verikoukis, C. (2023). Multi-Service Network Slicing 5G NR Orchestration via Tailored HARQ Scheme Design and Hierarchical Resource Scheduling. *IEEE Transactions on Vehicular Technology*, *72*(4), 5021–5034. https://doi.org/10.1109/TVT.2022.3223252

[12] Mhaske, S., Kee, H., Ly, T., Aziz, A., & Spasojevic, P. (2017). FPGA-Based Channel Coding Architectures for 5G Wireless Using High-Level Synthesis. *International Journal of Reconfigurable Computing*, *2017*, 1–23. https://doi.org/10.1155/2017/3689308

[13] Moges, T. H., Lakew, D. S., Nguyen, N. P., Dao, N.-N., & Cho, S. (2023). Cellular Internet of Things: Use cases, technologies, and future work. *Internet of Things*, *24*, 100910. https://doi.org/10.1016/j.iot.2023.100910

[14] Morais, D. H. (2024). 5G NR Overview and Physical Layer. In D. H. Morais, *Key 5G/5G-Advanced Physical Layer Technologies* (pp. 233–321). Springer International Publishing. https://doi.org/10.1007/978-3-031-57426-9_10

[15] Mulani, A. O., Warade, N. S., Khalaf, O. I., Bsoul, Q., Waghole, D., Jadhav, M., Jadhav, V. S., Bennour, A., Zawaideh, F., Alsekait, D. M., & AbdElminaam, D. S. (2025). Resource management optimisation of OFDM-IDMA system for 5G multi-tier backhaul networks. *Egyptian Informatics Journal*, *31*, 100756. https://doi.org/10.1016/j.eij.2025.100756

[16] Omri, A., Hernandez Fernandez, J., & Di Pietro, R. (2025). A Spectral and Energy Efficient Transmission Scheme for OFDM-based Communication Systems. *Computer Networks*, *260*, 111101. https://doi.org/10.1016/j.comnet.2025.111101

[17] Pathak, P., & Bhatia, R. (2025). Investigation of LDPC codes with interleaving for 5G wireless networks. *Annals of Telecommunications*, *80*(7–8), 569–579. https://doi.org/10.1007/s12243-024-01054-0

[18] Pyatin, I., Boiko, J., Eromenko, O., & Parkhomey, I. (2023). Implementation and analysis of 5G network identification operations at low signal-to-noise ratio. *TELKOMNIKA (Telecommunication Computing Electronics and Control)*, *21*(3), 496. https://doi.org/10.12928/telkomnika.v21i3.22893

[19] Pyatin, I., Boiko, J., Kovtun, V., & Kovtun, O. (2025). Radio frequency interface quality assessment in 4G/5G: Effects of IQ imbalance, phase noise, and nonlinearities on error vector magnitude. *PLOS One*, *20*(5), e0324170. https://doi.org/10.1371/journal.pone.0324170

[20] Ren, B., Teh, K. C., An, H., & Gunawan, E. (2024). MIMO-OFDM Modulation Classification Using 4D2DConvNet for 5G Communications. *IEEE Wireless Communications Letters*, *13*(7), 1883–1887. https://doi.org/10.1109/LWC.2024.3394708

[21] Santos, R., Castanheira, D., Silva, A., & Gameiro, A. (2024). Pipelined Multi-User IR-HARQ Scheme for Improved Latency Performance in URLLC. *IEEE Access*, *12*, 33473–33485. https://doi.org/10.1109/ACCESS.2024.3371994

[22] Shammaa, M., Mashaly, M., & El-mahdy, A. (2024). The Use of Deep Learning Techniques in OFDM Receivers for 5G NR: A Survey. *Procedia Computer Science*, *231*, 32–39. https://doi.org/10.1016/j.procs.2023.12.154

[23] Wang, Q., Cai, S., Chen, L., & Ma, X. (2020). A Throughput-Enhanced HARQ Scheme for 5G System via Partial Superposition. *IEEE Communications Letters*, *24*(10), 2162–2166. https://doi.org/10.1109/LCOMM.2020.3004407

[24] Yeh, H.-G. (2015). Architectures for MIMO-OFDM Systems in Frequency-Selective Mobile Fading Channels. *IEEE Transactions on Circuits and Systems II: Express Briefs*, *62*(12), 1189–1193. https://doi.org/10.1109/TCSII.2015.2498300

[25] Zhou, Y., Zheng, Y., & Wang, Z. (2023). Fast Successive-Cancellation Decoding of 5G Parity-Check Polar Codes. *IEEE Communications Letters*, *27*(1), 37–40. https://doi.org/10.1109/LCOMM.2022.3217163

D.Sc. Eng. Juliy Boiko
e-mail: boykoym@khmnu.edu.ua

In 2002 he received a Ph.D. at the Institute of Electrodynamics of the National Academy of Sciences of Ukraine in the field of device design and development of methods for measuring electrical and magnetic quantities. In 2015, he received D.Sc. in Engineering at the State University of Telecommunications (Kyiv, Ukraine) in the field of signal reception, synchronization, signal processing in telecommunication systems. Currently, full professor of the Department of Telecommunications, Media and Intelligent Technologies, Khmelnytskyi National University.
Research includes issues related to the development of devices for the automation of devices and systems, the theory of coding, synchronization systems, diagnostics and signal processing.

https://orcid.org/0000-0003-0603-7827

Ph.D. Eng. Ilya Pyatin
e-mail: ilkhmel@ukr.net

Received his diploma of a specialist and a qualification of a radio engineer from the Khmelnytskyi Technological Institute (Ukraine) in 1992. In 1996 he received a PhD degree from the Vinnytsia Polytechnic Institute in the field of radio measurements. Until 2021, he worked as an associate professor at the Department of Telecommunications at Khmelnytskyi National University. Currently he work at the Faculty of Computer Engineering of the Khmelnytskyi Professional College of the National University "Lviv Polytechnic" (Ukraine). Scientific research includes issues related to the development of error-correcting coding and synchronization systems for modern mobile telecommunications.

https://orcid.org/0000-0003-1898-6755